Planet. Space Sci., Vol. 30, No. 10, pp. 985–998, 1982
Printed in Great Britain.

0032-0633/82/100985-14$03.00/0
Pergamon Press Ltd.

DETERMINATION OF THE MAGNETOSPHERIC CURRENT SYSTEM PARAMETERS AND DEVELOPMENT OF EXPERIMENTAL GEOMAGNETIC FIELD MODELS BASED ON DATA FROM IMP AND HEOS SATELLITES

N. A. TSYGANENKO and A. V. USMANOV
Institute of Physics, Leningrad State University, Leningrad 198 904, U.S.S.R.

(*Received* 20 *November* 1981)

Abstract—An elaborate analytical model representation of the magnetospheric magnetic field has been developed based on the merged IMP–HEOS experimental data set. As distinct from the approach of Mead and Fairfield (1975), our model incorporates separate mathematical description of the ring current, the magnetotail current sheet and the magnetopause contributions to the total magnetic field. Model formulae for the magnetic field components contain in total 28 input parameters (21 linear coefficients and 7 non-linear parameters) obtained by means of an iterative minimization procedure, which fits the model to the experimental data sets corresponding to different levels of geomagnetic activity, as well as to different conditions in the solar wind.

1. INTRODUCTION

A considerable amount of accumulated measurements data provides at present a possibility to model the contribution of the extraterrestrial current systems to the magnetospheric magnetic field by means of direct fitting the model parameters to experimental data sets. Mead and Fairfield (1975) have developed a model based on a large set of the magnetic field data obtained from four IMP satellites during the period 1966–1972. The model is very simple mathematically, it is valid up to distances 10–15Re and allows to take into account the degree of magnetospheric disturbancy specified by the value of K_p-index. At the same time, the following shortcomings of the model have been pointed out by its authors. Firstly, the experimental data set lacks measurements in the high-latitude distant magnetosphere. Secondly, due to extreme simplicity of model functions approximating the measured external field distribution by quadratic polynomials of coordinates, the model current system derived from rot **B** has only a faint resemblance with that observed experimentally. By the same reason the model over-estimates the total field magnitudes in the high-latitude regions, showing at the same time too low values of B near the inner edge of the plasma sheet (Hedgecock and Thomas, 1975).

In the present paper we report the results of the development of an experimental geomagnetic field model based on the merged data set, including 12616 vector field averages obtained by IMP satellites (the Mead–Fairfield initial data set), complemented by the data from HEOS-1 and -2 spacecrafts, which consist of about 6000 vector averages. Due to elongation of HEOS orbits towards higher latitudes (Hedgecock and Thomas, 1975), we obtain thus a significant contribution from measurements in the polar magnetospheric regions and hence, a more uniform and complete spatial coverage is achieved in the merged data set.

We suggest also an improved set of model formulae providing the quantitative representation of the external magnetic field distribution. The expressions are rather simple from the computational point of view and contain less than thirty model parameters. At the same time, as distinct from the approach of Mead and Fairfield (1975), we retain a separate description of contributions from current systems having essentially different spatial structure. This enables us to model quantitatively the most important observed features of the ring current and the magnetotail current sheet.

At last, besides having sorted the data in accordance with the level of ground geomagnetic activity specified by the values of K_p, we have derived the model parameters corresponding to different conditions in the solar wind, based on King's (1977) data on the interplanetary magnetic field, velocity and particle density.

A detailed description of the spacecraft experiments and data distribution has been published elsewhere (Mead and Fairfield, 1975; Hedgecock and Thomas, 1975), so we can omit this point and turn directly to the question of quantitative representation of the magnetic field from extraterrestrial current systems.

2. MODEL APPROXIMATION FORMULAE

2.1 *Magnetic field of the ring current*

Assuming the ring current to be axially symmetric, let us consider the current and magnetic field distribution in a cylindrical geomagnetic coordinate system $\{\rho, \varphi, z\}$, with the z-axis antiparallel to the geodipole magnetic moment vector. We introduce the following distribution of the magnetic vector potential $\mathbf{A} = (0, A_\varphi, 0)$:

$$A_\varphi = C\rho(\rho^2 + z^2 + 4\rho_o^2)^{-3/2}. \tag{1}$$

The only difference between (1) and the corresponding expression for the purely dipolar vector potential is an additional term $4\rho_o^2$ in the brackets, which eliminates the singularity in the origin of coordinates. At large distances, i.e. with $\rho \gg \rho_o$ and/or $z \gg \rho_o$, the vector potential (1) corresponds to a dipolar source near the origin and provides thus a nearly current-free magnetic field, whereas at $r = (\rho^2 + z^2)^{1/2} \lesssim 2\rho_o$ we have a continuous axisymmetric ring-like current distribution with a characteristic radius of the order of ρ_o. From (1) we obtain the magnetic field components

$$B_\rho = B_o \frac{12\rho' z'}{(\rho'^2 + z'^2 + 4)^{5/2}} \tag{2}$$

and

$$B_z = 4B_o \frac{2z'^2 - \rho'^2 + 8}{(\rho'^2 + z'^2 + 4)^{5/2}} \tag{2a}$$

where the constant C is expressed in terms of the magnitude of the field depression B_o near the Earth and the coordinates are measured in units of ρ_o: $\rho' = \rho/\rho_o$, and $z' = z/\rho_o$.

The distribution of the current density in the plane of meridional cross-section, calculated from (2) and (2a) by taking rot $\mathbf{B}$, is shown in Fig. 1 as a family of current density isolines (in arbitrary units), which satisfactorily corresponds in its gross features to the generally accepted concept of the ring current. Figure 2 shows the plots of the current density and B_z obtained from (2, 2a) in the equatorial plane, vs geocentric distance ρ'; the maximum of j is seen to be located at $\rho' \approx 0.8\rho_o$ and the magnitude of the field depression increases monotonically towards the Earth. The last feature agrees with the experimentally deduced behaviour of the quantity ΔB in the inner magnetosphere (Sugiura, 1973). It can be seen also from Fig. 1, that the model ring current distribution is localized near equatorial plane, in accordance with the idea of "equatorial current sheet" developed by Sugiura (1972) as an explanation for the observed ΔB pattern. The proposed analytical representation of the ring current contribution contains only two parameters, ρ_o and B_o, and combines mathematical simplicity with its capability to model the main observed features.

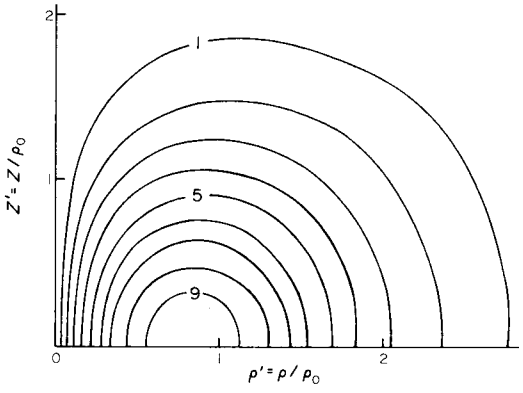

FIG. 1. A PATTERN OF CURRENT DENSITY ISOLINES IN THE MERIDIONAL CROSS-SECTION OF THE MODEL RING CURRENT. The isolines are labelled in arbitrary units.

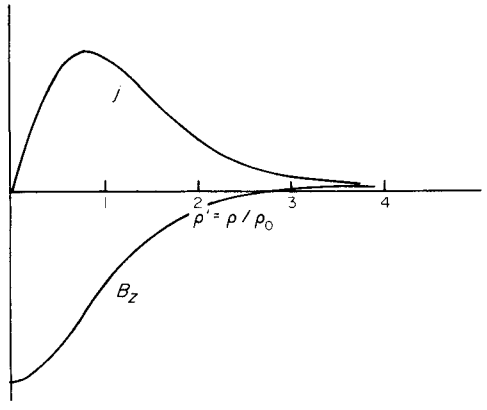

FIG. 2. A PROFILE OF THE RING CURRENT DENSITY AND THE VERTICAL MAGNETIC FIELD COMPONENT IN THE EQUATORIAL PLANE VERSUS RADIAL DISTANCE IN UNITS OF ρ_o.

2.2. *Magnetic field from the magnetotail currents*

Mathematical difficulties, which arise in mode-

ling the magnetotail current system by infinitely thin sheets, or by sheets of finite thickness with discontinuities of the volume current density, are well-known (e.g. Sergeev and Tsyganenko, 1980); we overcome this problem in the following way. Let us consider the current sheet as a superposition of infinite number of straight current filaments lying in the equatorial plane and being parallel to the y-axis. Each filament is supposed to have such an axially symmetric current distribution, that its magnetic field varies with radial distance R from the filament axis, located at $x = x_o$, as

$$dB \sim \frac{R/D}{1+(R/D)^2} = D\frac{[(x-x_o)^2+z^2]^{1/2}}{(x-x_o)^2+z^2+D^2},$$

where D is a scale half-thickness of the filament. Introducing the function $I(x_o)$ defining the plasma sheet current distribution along the magnetotail, we have in components

$$\begin{aligned} dB_x &= z[(x-x_o)^2+z^2+D^2]^{-1} \\ &\quad \times (2I(x_o)/c)\,dx_o \\ dB_z &= -(x-x_o)[(x-x_o)^2+z^2+D^2]^{-1} \\ &\quad \times (2I(x_o)/c)\,dx_o. \end{aligned} \tag{3}$$

Magnetic field produced by the whole sheet at an arbitrary point of space (x, z) (dependence on the y-coordinate will be introduced later on) can be obtained by integrating (3) with x_o from the inner $(x_o = x_N)$ up to the outer $(x_o = x_F)$ edge of the current slab. The spacecraft data set does not contain a significant amount of experimental points beyond $x_{GSM} = -20Re$ and hence, it is quite enough to restrict our model with a linear approximation for the function $I(x_o)$, leading to rather simple analytical expressions for the magnetic field components. The quantity $I(x_o)$ corresponds to the current per unit length of the sheet along the tail; rewriting it in terms of equivalent magnetic field $B(x_o)$, we have

$$I(x_o) = (c/2\pi)B(x_o) = (c/2\pi) \times \left(B_N + \Delta B\,\frac{x_0 - x_N}{S}\right), \tag{4}$$

where $S = x_N - x_F$.

Before writing down explicit formulae resulting from integration of (3) with the current function (4), we note that the proposed model contains neither singularities, nor discontinuities of the volume current density; however, it has infinite extension in the y-direction. This feature can lead to serious discrepancies between model results and measurements in the dawn and dusk regions of the near magnetotail (Willis and Pratt, 1972). A simple and effective way out is to multiply right hand sides in (3) by an even function of y, having the maximum at $y = 0$ and decreasing to zero with $|y| \to \infty$ on a scale width $y \sim 15Re$ of the order of magnetospheric radius in the dawn–dusk sectors. This modification does not violate the condition $\mathrm{div}\,\mathbf{B} = 0$ and the current flow line geometry shows in such a case much closer resemblance with that deduced from magnetic field observations.

Now we give the final model expressions for the magnetotail contribution to the total fileld (all the coordinates and field components refer to the solar magnetospheric coordinate system GSM; model simulation of the geodipole tilt effects will be discussed below):

$$\begin{aligned} B_x &= \left[\frac{z}{\pi(z^2+D^2)^{1/2}}\left(B_N - \frac{x_N - x}{S}\Delta B\right)\right. \\ &\quad \left. \times F(x,z) + \frac{\Delta B}{2\pi S}\,zG(x,z)\right] f(y) \\ B_y &= 0 \\ B_z &= \left[\left(B_N - \frac{x_N - x}{S}\Delta B\right)\frac{G(x,z)}{2\pi} + \frac{\Delta B}{\pi}\right. \\ &\quad \left. \times \left(1 - \frac{(z^2+D^2)^{1/2}}{S}F(x,z)\right)\right] f(y) \end{aligned} \tag{5}$$

where

$$\begin{aligned} F(x,z) &= \arctan\frac{x_N - x}{(z^2+D^2)^{1/2}} \\ &\quad - \arctan\frac{x_N - x - S}{(z^2+D^2)^{1/2}} \\ G(x,z) &= \ln\frac{(x_N - x)^2 + z^2 + D^2}{(x_N - x - S)^2 + z^2 + D^2} \\ f(y) &= [1 + (y/\Delta y)^2]^{-1}. \end{aligned}$$

Figure 3a shows the current flow line pattern in the equatorial plane, derived from (5) by taking rot **B**, with $D = 2Re$, $\Delta y = 10Re$, $S = 20Re$ and $x_N = -7Re$. In the next Fig. 3b we have plotted the projections of the current flow lines near $x = -10Re$ on the yz-plane. Introducing the factor $f(y)$ in (5), as is evident from the pictures, modifies the

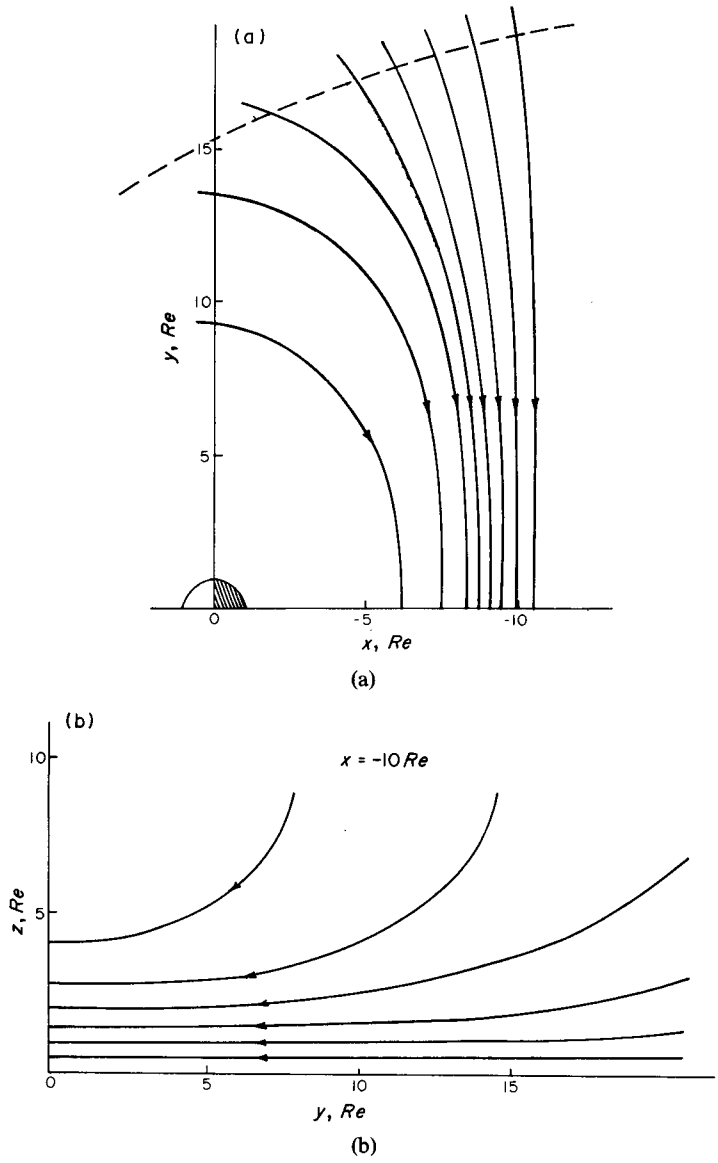

FIG. 3. CURRENT FLOW LINES IN THE MODEL MAGNETOTAIL CURRENT SHEET: (a) IN THE EQUATORIAL PLANE, (b) VIEW IN PROJECTION ON THE MAGNETOTAIL CROSS-SECTION.

current geometry in such a way, that a gradual transition from straight to nearly circular flow lines is observed, as we move from the tail towards the Earth (Fig. 3a); at the same time the current lines take an arched shape in projection on the tail crosssection with the convex towards equatorial plane (Fig. 3b). Both these features have been demonstrated to be typical to the magnetotail current geometry, as obtained form direct magnetic measurements (Hruska, 1971; Speiser and Ness, 1967); an indirect evidence for the same pattern stems from the particle distribution data (Hones, 1968).

An account for the geodipole tilt influence at the geometry of the intra-magnetospheric currents is based in the present model on the assumptions that (i) the ring current attitude is controlled entirely by the orientation of the Earth's magnetic moment, so that always $\mathbf{M}_{RC} \| \mathbf{M}_E$ and (ii) the magnetotail current sheet experiences a shift in the

z-direction by $z_s = r_H \sin\psi$; we have thus to substitute $z_r = z - z_s$ in (5) instead of z in case of $\psi \neq 0$. The last point is quite similar to Alekseev and Shabansky's (1972) approach to the simulation of the tilt-related effects. The model parameter r_H is the "hinging distance" (Bowling and Russell, 1973) defining the amplitude of the current sheet diurnal and seasonal oscillation.

2.3. *Magnetopause current contribution and the averaged magnetic effect of field-aligned currents*

Magnetic field from the magnetopause currents has the largest spatial variation scale in comparison with the other sources, which facilitates the choice of fitting functions. In particular, the same power series expansions, as those in the Mead–Fairfield model, can be applied. However, it is impossible to obtain in this case an accurate representation of the observed field distribution at distances beyond $x \sim -10Re$ due to non-monotonic behaviour of polynomials. For this reason we have chosen a polynomial approximation only in respect to y- and z-dependence, having combined it with exponential factors $\exp(x/\Delta x)$ which provide a satisfactory fitting to the data both in the dayside magnetosphere and at large distances in the tail region:

$$\begin{aligned}
B_x &= z(a_1 + a_2 \exp(x/\Delta x)) \\
&\quad + \sin\psi(a_3 + a_4 \exp(x/\Delta x) + a_5 y^2 + a_6 z^2) \\
B_y &= yz(b_1 + b_2 \exp(x/\Delta x)) \\
&\quad + y \sin\psi(b_3 + b_4 \exp(x/\Delta x)) \\
B_z &= c_1 + c_2 \exp(x/\Delta x) + y^2(c_3 + c_4 \exp(x/\Delta x)) \\
&\quad + z^2(c_5 + c_6 \exp(x/\Delta x)) \\
&\quad + z \sin\psi(c_7 + c_8 \exp(x/\Delta x)).
\end{aligned} \tag{6}$$

The dependence on the geodipole tilt angle, ψ, is represented in (6) by terms containing $\sin\psi$, rather than by terms linear in ψ, as in the fitting polynomials of Mead and Fairfield. Formally, our approximation is more correct, since the asymmetry effects should reach the maximum by $\psi = 90°$; practically, however, we have $|\psi| \lesssim 35°$ and thus, the difference is not significant. We note here that coordinates and magnetic field components in (6) refer to the solar–magnetic system SM.

The representation (6) contains 19 model parameters, from which 18 enter the expressions linearly, i.e. as coefficients; the non-linear parameter Δx is a characteristic length defining the gradient of the large-scale part of the external magnetic field. Imposing the condition $\mathrm{div}\,\mathbf{B} = 0$, we obtain four equations

$$\begin{aligned}
a_2/\Delta x + b_2 + 2c_6 &= 0 \\
a_4/\Delta x + b_4 + c_8 &= 0 \\
b_1 + 2c_5 &= 0 \\
b_3 + c_7 &= 0
\end{aligned} \tag{7}$$

which reduce the number of independent linear parameters to 14.

Like in the Mead and Fairfield (1975) approach, we have not imposed the condition $\mathrm{rot}\,\mathbf{B} = 0$ and hence, the expansions (6) can in principle account for the magnetic effects from the rest of the intramagnetospheric currents, which for some reasons cannot be reproduced properly by (2, 2a) and (5); in particular, this pertains to the field-aligned currents. In the work by Tsyganenko and Suslikov (1981) it is shown that the field-aligned currents can provide a significant contribution to the large-scale magnetospheric magnetic field; in the dayside sector this results in a substantial displacement of polar cusps and of the magnetopause. It should be understood, however, that only spatially averaged gross features of field-aligned current contribution can be accounted for by our fitting functions (6). A more detailed study requires more complex model, as well as more extended and refined data sets.

3. RESULTS AND DISCUSSION

The total model magnetic field produced by extraterrestrial sources is obtained by taking a sum of (2, 2a), (5) and (6), after having done the proper coordinate transformations. A model version is defined completely by setting numerical values to 28 input parameters; seven of them (ρ_o, D, x_N, r_H, S, Δy and Δx) enter in the expressions non-linearly. As to the linear coefficients (a_1–a_6, b_1–b_4, c_1–c_8, B_N, ΔB and B_o), only 17 of them are independent; four coefficients c_5–c_8 are determined from the constraint equations (7).

Derivation of independent parameters was carried out by means of an iterative scheme; at each step we first compute all the linear coefficients using a least squares procedure and then find the non-linear parameters by a version of the consecutive descent method, minimizing the r.m.s. deviation of the model field from the experimental data set

$$\sigma = \left[\sum_{j=1}^{N} (\mathbf{B}_{\mathrm{mod}}^{(j)} - \mathbf{B}_{\mathrm{exp}}^{(j)})^2/N\right]^{1/2}.$$

Computations have shown that the most significant decrease of σ occurs in the first 3–4 iterations, only minor changes being observed at the next steps. For this reason, we have decided to finish computer runs in the 4th approximation. Also, it appeared difficult to obtain the best fit values for two non-linear parameters, basing solely on the present data sets; these are the ring current parameter, ρ_o and the length of the tail current sheet, S. The most likely reason for difficulties with ρ_o is the lack of experimental points in the near-Earth region with $r \lesssim 5Re$. Besides that, in the inner magnetosphere the magnetic effect of the ring current is rather similar to that of the tail current sheet, which leads to an unstable behaviour of model parameters and poorer convergence of iterations, unless ρ_o is fixed. The parameter S has no clear physical meaning at all; its choice should be made taking into account the spatial extension of the modeling region in the tailward direction. All these considerations, together with the computer time limitations, lead us to the decision to fix ρ_o and S with the values $4Re$ and $50Re$, respectively. As computations have shown, we obtain in such a case quite reasonable values of the magnetic moment of the model ring current $M_{RC} \sim 0.25M_E$, in agreement with the earlier estimates (Schield, 1969).

Formation of initial data sets, corresponding to different levels of ground geomagnetic disturbancy has been carried out in such a way that, on the one hand, a sufficiently detailed resolution in K_p has been achieved. On the other, the number of experimental points in each set is large enough, ensuring thus sufficient reliability of results. The following values of K_p were adopted for sorting the data: 0; 0+; 1−; 1; 1+; 2−; 2; 2+; 3−; 3 and 3+; >3+ (average K_p value for the last interval being 4+).

Results of fitting the model parameters to the data sets are listed in Table 1; each column corresponds to one of the above K_p values or intervals. The following quantities are given in the columns (from the top): the value of K_p-index, the number of points in the data set (N), the r.m.s. deviation of the model field from the data (σ), 18 coefficients for the expansions (6), two linear parameters of the magnetotail current sheet (B_N and ΔB), the ring-current depression (B_o) and five non-linear parameters (Δx, x_N, D, Δy and r_H). Two non-linear parameters, S and ρ_o, as already noted above, were kept constant in all cases ($S = 50Re$, $\rho_o = 4Re$) and are not included in the Table.

In Fig. 4 the plots of the model parameters Δx, Δy, x_N, r_H and D vs K_p are given; Fig. 5 shows the behaviour of the ring current parameter, B_o and the r.m.s. deviation, σ. The last two quantities reveal the most ordered variation. The σ curve rises almost monotonically from $\sigma = 7.52$ for $K_p = 0$ up to $\sigma = 18.94$ for $K_p > 3+$. These values are very close to the corresponding results obtained by Mead and Fairfield (1975) for the same K_p, in spite of the fact, that a significantly more extended data sets were used in our analysis, with the maximum geocentric distance to the measurement points exceeding $30Re$, whereas the Mead–Fairfield data are restricted by $r \lesssim 17Re$. This result seems to speak in favor of our model approximation formulae. To check this suggestion more quantitatively, we have computed the coefficients of the Mead–Fairfield quadratic polynomials providing the best fit to the present data set with $K_p > 3+$. The r.m.s. deviation value has increased in this case to $\sigma = 23.82$, i.e. by 25% against our result.

The ring current parameter, B_o, as should be expected, shows a clear tendency to increase with rising K_p, from -12.5 nT for $K_p = 0$, up to -48.1 nT for $K_p > 3+$. Of all non-linear parameters (Fig. 4), only the current sheet half-

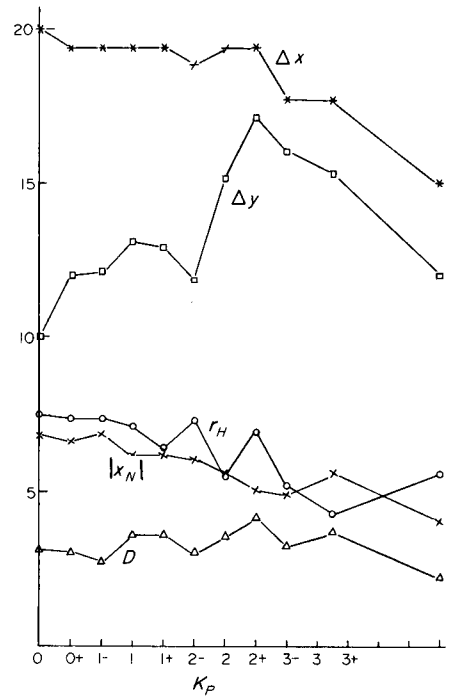

FIG. 4. PLOTS OF FIVE NON-LINEAR MODEL PARAMETERS VERSUS K_p-INDEX.

TABLE 1.

K_p	0	0+	1−	1	1+	2−	2	2+	3−	3, 3+	>3+
N	634	1553	1784	1754	1972	1836	1654	1618	1398	2286	2375
σ	7.52	8.55	10.14	10.87	11.44	12.18	11.91	13.58	12.80	15.79	18.94
a_1	−0.0922	−0.350	−0.467	−0.654	−0.235	−0.666	−1.01	−1.07	−0.652	−1.88	−1.17
a_2	1.27	1.47	1.73	1.98	1.66	2.24	2.62	2.69	2.48	4.02	3.65
a_3	26.5	15.2	20.3	11.6	25.0	16.4	5.48	17.8	7.25	−1.45	0.912
a_4	−14.2	−7.24	−13.4	−7.96	−14.7	−6.94	−2.37	−7.32	−1.81	1.19	8.01
a_5	−0.0238	−0.0320	−0.0160	0.0108	−0.0257	−0.00335	0.0375	−0.00876	0.0139	0.0115	0.0758
a_6	0.0294	0.0445	0.0425	0.0696	0.0621	0.0748	0.0867	0.0247	0.0942	0.196	0.190
b_1	−0.0265	0.0199	0.0281	0.0289	0.0334	0.0552	0.0355	0.0260	0.0332	0.00914	0.0615
b_2	−0.0362	−0.103	−0.126	−0.129	−0.140	−0.183	−0.148	−0.140	−0.163	−0.156	−0.257
b_3	−1.09	−0.441	−0.417	−0.116	−0.275	−0.0438	−0.233	−0.137	−0.630	0.623	0.168
b_4	0.00922	−1.07	−1.39	−1.61	−1.61	−2.33	−1.73	−1.68	−1.48	−2.98	−3.40
c_1	−29.8	−15.4	−21.5	−18.2	−22.7	−18.8	−19.8	−18.5	−18.4	−17.8	−17.8
c_2	34.2	26.5	34.4	33.2	32.6	31.7	36.1	34.4	32.3	40.1	32.5
c_3	0.157	0.0564	0.0928	0.0515	0.0673	0.0472	0.0679	0.0416	0.0770	0.0595	0.0692
c_4	−0.137	−0.0499	−0.103	−0.0578	−0.0643	−0.0421	−0.0835	−0.0478	−0.0730	−0.0792	−0.0658
c_5	0.0133	−0.00997	−0.0140	−0.0145	−0.0167	−0.0276	−0.0177	−0.0130	−0.0166	−0.00457	−0.0308
c_6	−0.0128	0.0137	0.0185	0.0136	0.0275	0.0322	0.0066	−0.00107	0.0118	−0.0347	0.00661
c_7	1.09	0.441	0.417	0.116	0.275	0.0438	0.233	0.137	0.630	−0.623	−0.168
c_8	0.68	1.44	2.08	2.02	2.37	2.69	1.85	2.07	1.58	2.91	2.86
B_N	46.6	43.5	51.5	56.8	65.0	63.1	61.7	68.8	61.9	79.1	82.6
ΔB	104.0	62.9	83.5	81.1	121.0	101.0	90.1	98.2	86.2	105.0	124.0
B_o	−12.5	−21.0	−24.9	−26.6	−30.8	−29.1	−40.0	−32.3	−35.2	−46.2	−48.1
Δx	20.00	19.44	19.44	19.44	19.44	18.89	19.44	19.44	17.78	17.78	15.00
x_N	−6.82	−6.52	−6.82	−6.22	−6.22	−6.07	−5.63	−5.04	−4.89	−5.63	−4.00
D	3.13	3.06	2.76	3.57	3.57	2.98	3.50	4.17	3.20	3.72	2.24
Δy	10.00	12.0	12.22	13.11	12.89	11.79	15.11	17.11	16.00	15.33	12.00
r_H	7.50	7.37	7.37	7.11	6.46	7.37	5.56	6.98	5.17	4.32	5.56

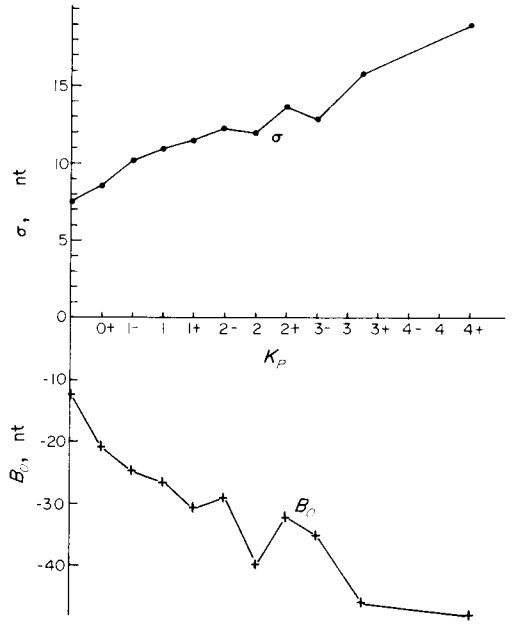

FIG. 5. PLOTS OF THE RING CURRENT PARAMETER B_0 AND OF THE r.m.s. DEVIATION OF THE MODEL FORM THE EXPERIMENTAL DATA VS K_p.

thickness, D, does not show any visible tendency to ordered changes with K_p; on the average, $D \approx 3.3Re$. A possible explanation is that during quiet periods the current sheet is relatively thick due to a more dipolar field line shape, whereas during substorms it thins down and then expands rapidly; on the average, however, its thickness remains approximately the same. As to the parameter x_N, a distinct earthward shift of the current sheet is evident from the corresponding plot for larger levels of disturbancy, from $x_N \approx -7Re$ for $K_p = 0$, up to $x_N \approx -4.5Re$ for $K_p > 3+$, in accordance with experimental results of the plasma sheet dynamics (Vasyliunas, 1968). The plot of r_H variation vs K_p is rather close to that of x_N, i.e. the hinging distance can be approximately identified with the distance to the inner edge of the current sheet and exhibits the same dependence on the geomagnetic activity. This feature is in line with the result obtained by Bowling and Russell (1973) from a statistical study of the current sheet geometry at $x_{GSM} \sim -30Re$.

The behaviour of the Δy parameter is somewhat more complex. In the range of K_p from 0 to 2+ Δy shows a general increase from $\Delta y \approx 10Re$ to $\Delta y \approx 17Re$ (the point with $K_p = 2-$ drops out) and then decreases up to $\Delta y \approx 12Re$ by $K_p > 3+$; it is of interest to note the obvious matching of the descending slope of Δy curve with that of the Δx parameter giving the variation length of the large-scale field from the magnetopause sources. The most likely interpretation of such behaviour may be as follows. The ascending slope of the Δy plot corresponds to an increase of the plasma sheet current (and hence, of the magnetotail cross-section) at initial stage of substorms, or during convection disturbances, manifested by only a weak increase in the ground activity ($K_p < 2$). The general compression of the magnetosphere is still relatively weak for this K_p interval and the corresponding Δx is large. For greater values of K_p we have to expect an increased contribution from measurements made during periods with higher solar wind pressure and therefore, a decrease in both scaling parameters, Δx and Δy.

An inspection of the linear parameters a_1–a_6, b_1–b_4, c_1–c_8, B_N and ΔB shows a lack of monotonous changes with K_p, as distinct from the Mead–Fairfield model (to a somewhat lesser extent this applies to B_N; a tendency to grow with K_p is obvious for this quantity). The main reason is a comparatively large number of model parameters. On the one hand, this ensures a higher flexibility of model representation, i.e. a capability to match accurately the details of the field distribution; on the other hand, it leads to a certain disadvantage, which is a higher sensitivity of the inverse problem solution with respect to random inhomogeneities in the experimental data coverage. It is unlikely to expect the distribution of the experimental information density in 4-dimensional space (x, y, z, ψ) to be similar enough for all data sets used in our study. These considerations clarify the origin of the above mentioned scatter in the values of linear parameters. At the same time, the total magnetic field distributions calculated from the obtained parameters should change with K_p in a more regular way. This is confirmed by Fig. 6, which shows a family of curves $B_z(x)$ representing the variation of the net contribution from all extraterrestrial sources along the x_{GSM} axis for $K_p = 0$; 1; 2; 3 and 3+; >3+. A gradual decrease of the near-Earth magnetic field is seen throughout the region $|x_{GSM}| \lesssim 6Re$ with increasing K_p. One of the shortcomings of the present model is evident also from Fig. 6, which is an over-estimation of B_z in the plasma sheet beyond the distance $x_{GSM} \sim -16Re$. At $x_{GSM} = -20Re$ the model external sources provide a positive contribution to B_Z, which is about 5 nT for $K_p < 2$. With account of the geodipole contribution, the total field magnitude is ~9 nT; this value is at least by 3–5 nT

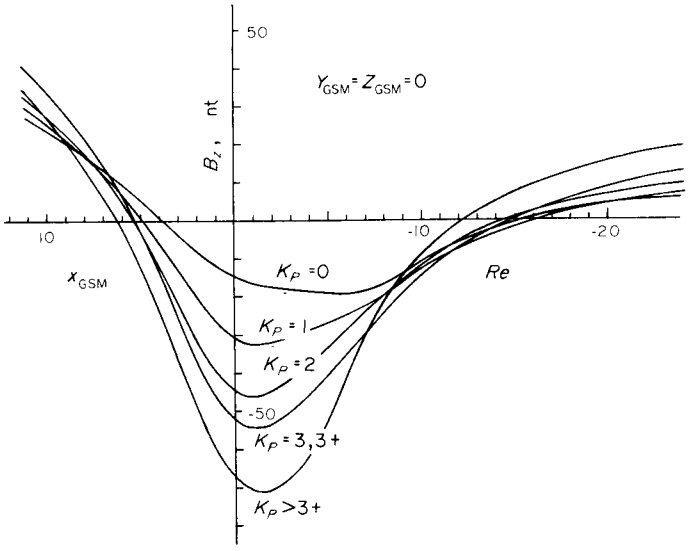

FIG. 6. FAMILY OF CURVES $B_z(x)$, SHOWING THE VARIATION OF THE EXTERNAL FIELD ALONG THE x_{GSM}-AXIS FOR DIFFERENT VALUES OF K_p.

higher than the average experimental estimate for quiet periods and for greater K_p the discrepancy is even larger. An obvious reason is the lack of data in the region $x_{GSM} \lesssim -16Re$, $|z_{GSM}| \lesssim 10Re$, since the IMP data set is limited by radial distances $r \lesssim 17Re$, whereas the HEOS data for $x_{GSM} \lesssim -15Re$ pertain only to the high-latitude magnetotail.

In Fig. 7 the curves of the total magnetic field variation (including the geodipole contribution) in the nightside model magnetosphere along the line $y_{GSM} = 0$, $z_{GSM} = 10Re$ are given for the same values of K_p. The plots exhibit a well-ordered monotonous dependence of the magnetotail magnetic field on the ground disturbancy level, being shifted upwards for higher K_p values. Note that the change in K_p from 0 to 1 is manifested mainly in the tailward part of the corresponding curve. This effect is evident already at $x_{GSM} = -10Re$, where the density of experimental points is large enough. We may suggest, hence, the feature to be physically meaningful; a possible interpretation is that a significant portion of data points with $K_p < 2$ refer to situations, typical for weak or developing substorms without intense ring current, but with a substantially increased tail currents.

Figures 8–10 demonstrate the results of field line tracing for selected versions of the proposed model. With the purpose of illustrating the effects of the K_p increase, we give examples for $K_p = 0$; 2; and $>3+$. As the plots show, our model in-

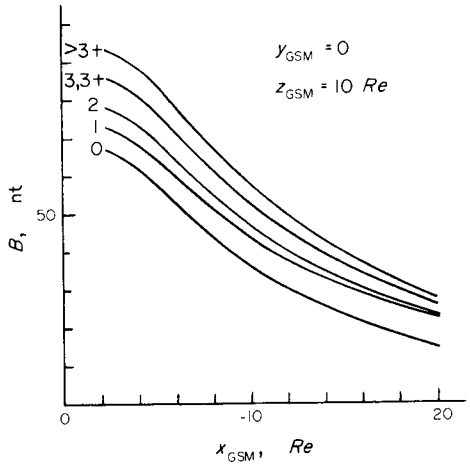

FIG. 7. FAMILY OF PLOTS FOR THE TOTAL MODEL MAGNETIC FIELD VARIATION ALONG THE LINE $Y_{GSM} = 0$, $Z_{GSM} = 10Re$.

corporates all the phenomena considered traditionally as the main effects accompanying the rising of substorm activity, which are (i) a decrease of the subsolar magnetopause distance, (ii) a "peeling" of the dayside field lines with a corresponding decrease of the polar cusps latitude, (iii) an enhanced stretching of the nightside field lines.

A detailed study of the magnetospheric model structure, mapping the ground-observed geophysical phenomena along force lines, an investigation

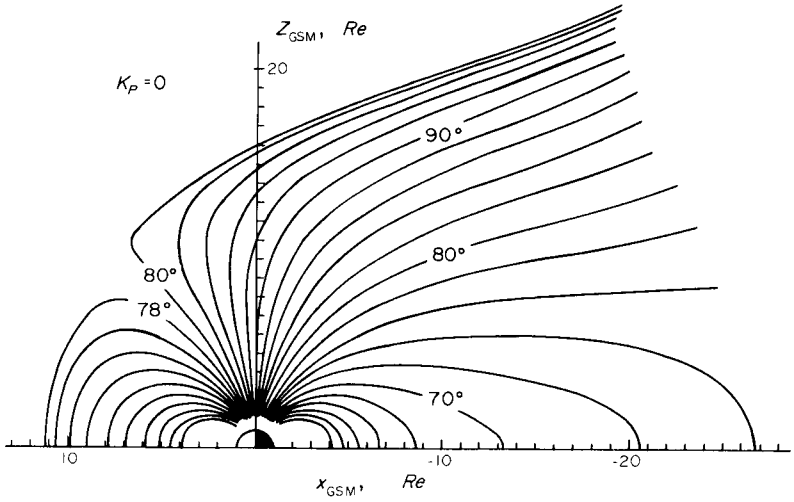

FIG. 8. A NOON-MIDNIGHT CONFIGURATION OF THE MODEL MAGNETIC FIELD LINES, IN THE VERSION WITH $K_p = 0$.

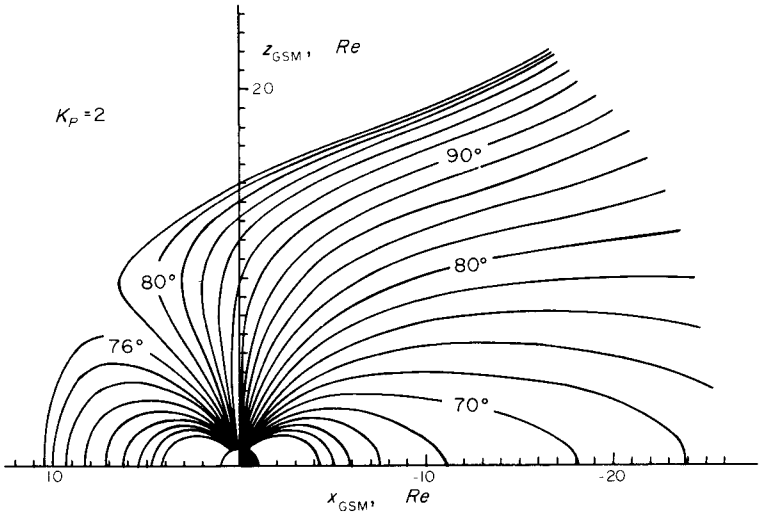

FIG. 9. THE SAME, AS IN FIG. 8, FOR $K_p = 2$.

of the asymmetry effects caused by the geodipole tilting and a comparison with other models and satellite data will be treated in a separate publication; here we confine ourselves only by showing in Fig. 11 a field-line configuration in the model version with $K_p = 1$, corresponding to the tilted geodipole ($\psi = 30°$).

4. THE INTERPLANETARY MAGNETIC FIELD EFFECTS

Turning now to the IMF-related phenomena, we show in Fig. 12 the magnetospheric configuration, which refer to the case with $K_p < 2$ and $B_z^{IMF} < 0$. The corresponding experimental data set was formed with the aid of King's (1977) interplanetary data tape. As can be seen from the figure, in spite of relatively low ground disturbancy level, the polar cusps map in this case to the latitude $\approx 77.5°$, whereas the model version without any IMF sorting (and for the same K_p interval) yields the value $\approx 79°$.

We have done a more refined analysis for the dayside sector only, having carried out a normalization of measured magnetic field components to a constant value of the solar wind dynamical pressure $p = nmv^2$. This correction has been per-

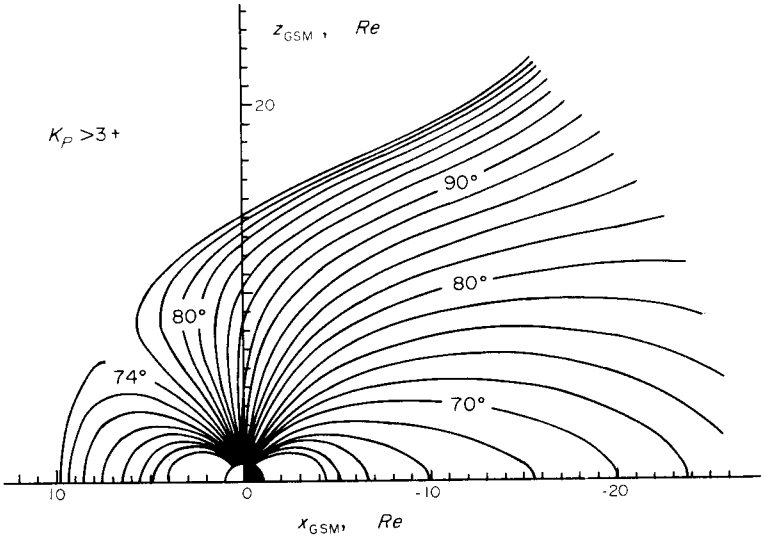

FIG. 10. THE SAME, AS IN FIG. 8, FOR $K_p > 3+$.

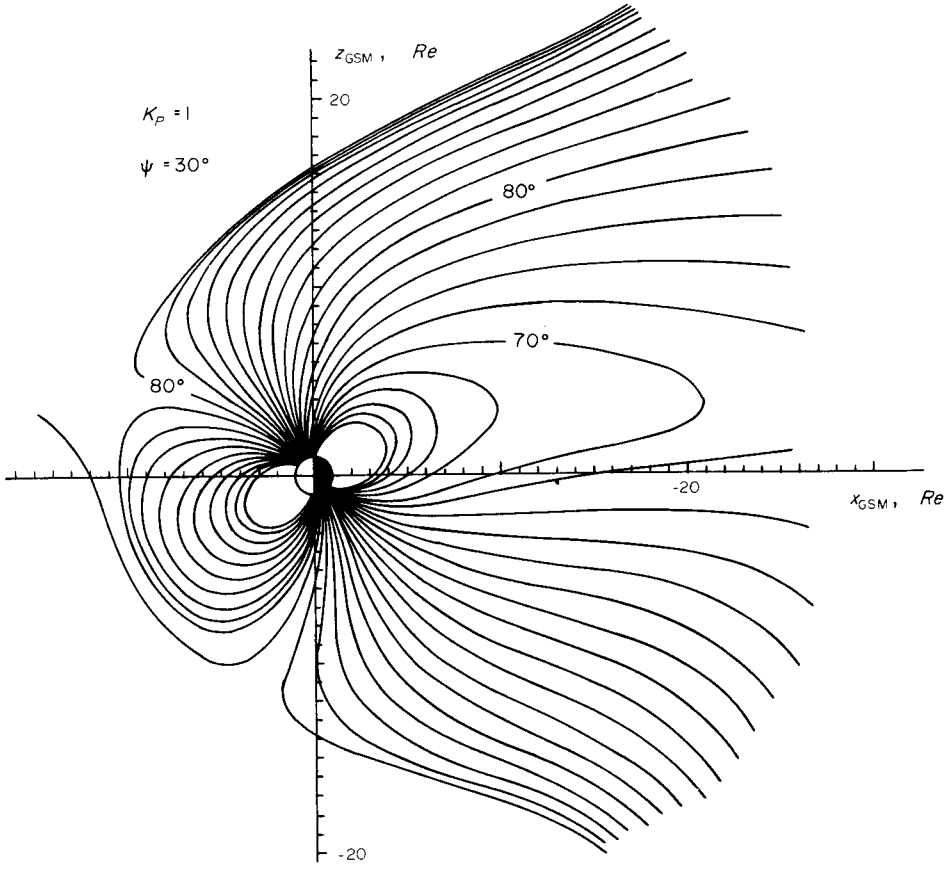

FIG. 11. CONFIGURATION OF THE MAGNETOSPHERIC MODEL FIELD LINES IN THE CASE OF TILTED GEODIPOLE; $\psi = 30°$.

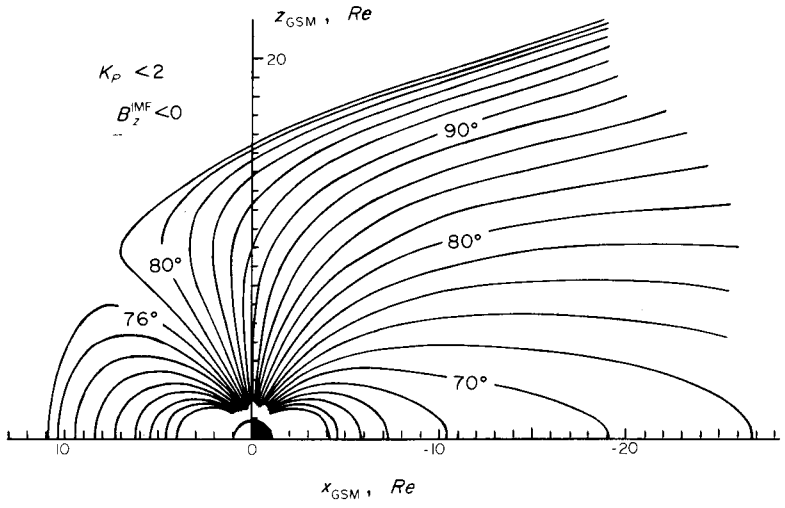

FIG. 12. THE SAME, AS IN FIG. 8, FOR $K_p < 2$ AND $B_z^{IMF} < 0$.

formed using the Choe–Beard (1974) representation of the magnetopause current contribution to the total field, which contains the solar wind pressure dependence in terms of model parameter $R_o = (M_E^2/4\pi nmv^2)^{1/6}$ and is able to account for the geodipole tilt effects. The measured values of the magnetic field components were corrected in such a way that

$$B_{x,y,z}^{norm} = B_{x,y,z}^{meas} + B_{x,y,z}^{C.-B.},$$

where $B_{x,y,z}^{C.-B.}$ are the correction terms, calculated from the second-order expansions of Choe and Beard and corresponding to the difference between actual pressure and its "standard" value $p = 2 \cdot 10^{-8}$ dynes cm^{-2}. Despite inevitable reducing of data sets due to gaps in the solar wind data, it still appeared possible to organize two data sets with about 700 experimental points in each one, corresponding to $B_z^{IMF} > 0$ and $B_z^{IMF} < 0$. Figure 13 shows two model curves representing the variation of external magnetic field along the x_{GSM} axis for the two polarities of B_z^{IMF}. An averaged effect of B_z^{IMF} reversal to the South is thus a general decrease of the intra-magnetospheric field in the dayside sector. The near-Earth depression deepens, most likely, due to an average increase of the ring current intensity, as a response to a larger geoefficiency of the solar wind streams with the southward B_z. At the same time, we observe also a distinct decrease of B near the subsolar magnetopause in case of $B_z^{IMF} < 0$. This effect surely

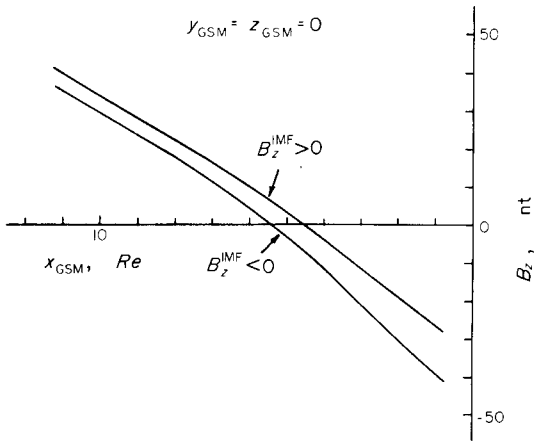

FIG. 13. VARIATION OF THE EXTERNAL MAGNETIC MODEL FIELD ALONG THE DAYSIDE PORTION OF THE x_{GSM}-AXIS FOR TWO POLARITIES OF INTERPLANETARY MAGNETIC FIELD. Corresponding model parameters have been computed from data sets normalized to the same value of the solar wind pressure, $p = 2 \cdot 10^{-8}$ dynes cm^{-2}.

cannot be ascribed to the ring current and hence, we have to look for other sources, the most likely candidates, in our opinion, being the field-aligned currents. Their intensity rises during periods with $B_z^{IMF} < 0$ (Iijima and Potemra, 1976) and as a model calculation has shown (Tsyganenko and Suslikov, 1981), the corresponding large-scale magnetic effect is large enough to produce a ~5 nT decrease of the total field near the subsolar point.

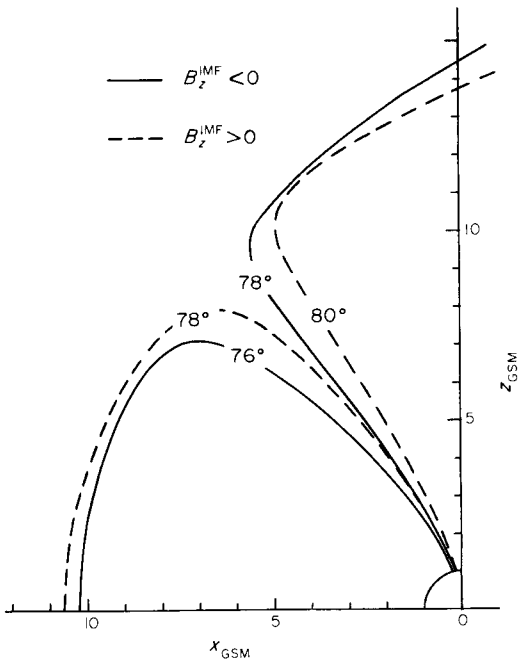

FIG. 14. CONFIGURATION OF THE DAYSIDE MAGNETIC FIELD LINES DELINEATING THE POLAR CUSP, FOR TWO POLARITIES OF B_z^{IMF}.

Just the same value of subsolar field reduction we observe in Fig. 13. Another equivalent interpretation of this phenomenon developed by Pudovkin and Semenov (1977) is based on an idea of partial penetration of the interplanetary magnetic field into the magnetosphere. A direct experimental foundation for such an approach has been discussed by Kovner and Feldstein (1973).

The last Fig. 14 shows the magnetic field lines in the vicinity of polar cusp corresponding to the same two cases with $B_z^{IMF}>0$ (dashed lines) and $B_z^{IMF}<0$ (solid lines). As can be seen from the plot, the average equatorward shift of the polar cusp projection caused by the IMF reversal to the south is about 2° in latitude; the corresponding earthward displacement of the magnetopause in the subsolar region is $\approx 0.4Re$.

5. SUMMARY

Based on the magnetospheric magnetic field data sets, which comprise in total about 19,000 vector averages pertaining to the outer magnetosphere and near magnetotail regions, we have developed an elaborate set of magnetospheric magnetic field models providing its numerical representation for different values of K_p index. A separate account of the contribution from different magnetospheric current systems has made it possible to track the K_p-dependence of their main physical parameters. The magnetic field data processing combined with their sorting in accordance with the solar wind state has allowed us to observe in the model field the main effects related to the polarity of B_z-component of the interplanetary magnetic field.

Acknowledgements—It is a great pleasure to thank Drs. G. D. Mead and D. H. Fairfield from Goddard Space Flight Center and Dr. P. C. Hedgecock from Imperial College, London, for providing us with the magnetic field data of IMP and HEOS spacecrafts. The IMP data, as well as the Interplanetary Medium Data tape have been set at our disposal by the National Space Science Data Center through the World Data Center A for Rockets and Satellites.

REFERENCES

Alekseev, I. I. and Shabansky, V. P. (1972). A model of a magnetic field in the geomagnetosphere. *Planet. Space Sci.* **20**, 117.

Bowling, S. B. and Russell, C. T. (1973). The position and shape of the neutral sheet at 30*Re*. *J. geophys. Res.* **81**, 270.

Choe, J. Y. and Beard, D. B. (1974). The compressed geomagnetic field as a function of dipole tilt. *Planet. Space Sci.* **22**, 595.

Hedgecock, P. C. and Thomas, B. T. (1975). HEOS observations of the configuration of the magnetosphere. *Geophys. J. R. astr. Soc.* **41**, 391.

Hones, E. W. (1968). Review and interpretation of particle measurements made by Vela satellites in the magnetotail, in *Physics of the Magnetosphere* (Carovillano, R. L. ed.), p. 392. D. Reidel, Dordrecht.

Hruska, A. (1971). Electric current system in the undisturbed magnetospheric tail. *Radio Sci.* **6**, 295.

Iijima, T. and Potemra, T. A. (1976). Field-aligned currents in the dayside cusp observed by Triad. *J. geophys. Res.* **81**, 5971.

King, J. H. (1977). *Interplanetary medium data book*: *Rept. NSSDC* 77-04a. Greenbelt.

Kovner, M. S. and Feldstein, Ya. I. (1973). On solar wind interaction with the Earth's magnetosphere. *Planet. Space Sci.* **21**, 1191.

Mead, G. D. and Fairfield, D. H. (1975). A quantitative magnetospheric model derived from spacecraft magnetometer data. *J. geophys. Res.* **80**, 523.

Pudovkin, M. I. and Semenov, V. S. (1977). Peculiarities of the MHD-flow by the magnetopause and generation of the electric field in the magnetosphere. *Ann. Geophys.* **33**, 423.

Schield, M. A. (1969). Pressure balance between solar wind and magnetosphere. *J. geophys. Res.* **74**, 1275.

Sergeev, V. A. and Tsyganenko, N. A. (1980). *The Earth's Magnetosphere.* Nauka, Moscow.

Speiser, T. W. and Ness, N. F. (1967). The neutral sheet

in the geomagnetic tail: its motion, equivalent currents and field line connection through it. *J. geophys. Res.* **72**, 131.

Sugiura, M. (1972). Equatorial current sheet in the magnetosphere. *J. geophys. Res.* **77**, 6013.

Sugiura, M. (1973). Quiet-time magnetospheric field depression at 2.3–3.6*Re*. *J. geophys. Res.* **78**, 3182.

Tsyganenko, N. A. and Suslikov, D. G. (1981). Large-scale magnetic effects of magnetospheric field-aligned currents, in *Magnetospheric Researches, No.* 2. Nauka, Moscow (in press).

Vasyliunas, V. M. (1968). A survey of low-energy electrons in the evening sector of the magnetosphere with OGO-1 and OGO-3. *J. geophys. Res.* **73**, 2839.

Willis, D. M. and Pratt, R. J. (1972). A quantitative model of the geomagnetic tail. *J. atmos. terr. Phys.* **34**, 1955.